A High-Transmission, Multiple Antireflective Surface Inspired from Bilayer 3D Ultrafine Hierarchical Structures in Butterfly Wing Scales

Zhiwu Han, Zhengzhi Mu, Bo Li, Shichao Niu, Junqiu Zhang, and Luquan Ren*

Antireflective surfaces have been proposed as a way to enhance the optical performance of photovoltaic devices, perhaps one of the most well-known example is solar cells.[1] In practical applications, suppressing reflection and improving transmission of light are crucial in developing high-performance optical elements. Up to now, there are two kinds of available approaches to obtain antireflective surfaces.[2] One is coating porous or multilayered films on the surface of devices. Among them, antireflective coatings (ARCs) with a gradient refractive index have been proved the most effective one in suppressing the Fresnel reflections at an interface.[3] The other is the subwavelength antireflective structures (ARSs) directly fabricated on surface of the devices. Although both ARC and ARS can impart a surface with antireflective property, there are some distinct disadvantages in ARC when compared to ARS, such as the control of coating conditions, the adhesive failure caused by thermal mismatch, and the poor interfacial adhesion.[4] In contrast, ARS exhibits higher mechanical stability and better durability due to the monolithic nanostructures and the homogeneous materials. In general, ARS is admittedly the reliable method to promote the performance of optical surfaces by increasing transmission, eliminating ghost images, or veiling glare.[5] In fact, ARS is incredibly abundant in nature that is a great art gallery involving diverse creatures and has provided enormous inspirations for scientists to explore novel materials with unique structures. The biological prototypes that scientists are most keen on mimicking include moth eyes,[6] fly eyes,[7] cicada wings,[8] butterfly wings,[9] and so forth. Among all of them, butterfly wings are probably the most typical and have attracted special attention due to their spontaneously arranged scales with complex ultrafine nanostructures that lead to an excellent multifunctional integrated optical system.[10] However, the multiple antireflective mechanism based on the bilayer 3D ultrafine hierarchical structures in butterfly wing scales has not been clearly understood and has not yet formed a unified conclusion.

Prof. Z. Han, Dr. Z. Mu, Dr. B. Li, Dr. S. Niu, Dr. J. Zhang, Prof. L. Ren
Key Laboratory of Bionic Engineering (Ministry of Education)
Jilin University
Changchun, Jilin 130022, P. R. China
E-mail: niushichao@jlu.edu.cn

DOI: 10.1002/smll.201502454

In order to fabricate antireflective surfaces, more and more material scientists and engineers have devoted themselves to develop and experiment with various advanced nanofabrication techniques, such as electron-beam lithography,[11] nanoimprint lithography,[12] holographic lithography,[13] fast atom beam etching,[14] colloidal lithography,[15] reactive ion etching.[16] Therefore, the ARS surfaces incorporating the high-throughput, broadband, and quasi-omnidirectional antireflective properties with different structures have been fabricated and characterized by many groups, such as paraboloid,[17] nanotip,[18] nanorod,[19] nanopillar,[2,20] nanograss,[21] nanocone,[22] pyramid texture,[23] nanowall,[24] etc. However, it is noted that the above-mentioned routes are not universal and just suitable for fabricating certain specific structures. The concomitant high cost could not be neglected as well. Moreover, the exact combination of bilayer 3D ultrafine hierarchical structures and cuticle complex refractive index of butterfly wing scales is beyond the capacity of existing nanofabrication techniques.[25] Therefore, developing a universal, low-cost, and effective biomimetic method to fabricate high-performance ARS should be taken seriously enough.

Herein, we reported a high-transmission, multiple antireflective surface inspired from bilayer 3D ultrafine hierarchical structures in butterfly *Trogonoptera brookiana* wing scales. A facile wet chemical biomimetic fabrication method combining sol–gel and selective etching processes was adopted to generate the biomimetic high-transmission antireflective replicas with nanoditch array structures. The morphologies and dimensions of the nanostructures in both original wing scales and SiO_2 biomimetic replicas were characterized by optical microscope, field emission scanning electron microscope (FESEM), and transmission electron microscopy (TEM). The antireflective properties of the fabricated biomimetic replicas were evaluated by reflectance spectra and transmittance spectra. Encouragingly, not only the ultrafine hierarchical structures but also the excellent antireflective properties of original wing scales were well preserved through regulating reaction conditions. Furthermore, the underlying multiple antireflective mechanisms based on the bilayer 3D ultrafine hierarchical structures of butterfly wing scales and the nanoditch array structures of the biomimetic replicas were fully revealed from the multicoupling perspectives.

In this work, the wingspan of male butterfly *Trogonoptera brookiana* is about 125.2 mm. The triangle green patches on the fore and hind wings can be identified clearly (**Figure 1**a,c).

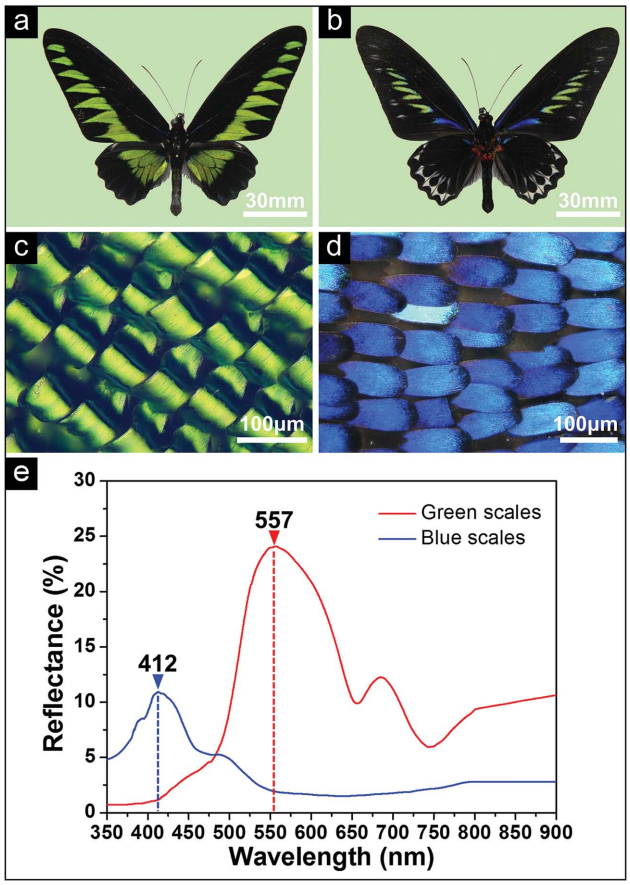

Figure 1. a,b) Macroscopic digital pictures of intact male *Trogonoptera brookiana* butterfly exhibiting brilliant structure colors; c,d) 3D stereoscopic microscope images of green scales and blue scales; e) reflectance spectra of green scales and blue scales at normal incidence.

The narrow blue patches on the reverse side are close to the root segments of the fore wings and demonstrate gorgeous metallic blue color (Figure 1b,d). As expected, the reflectance spectra of green scales and blue scales (Figure 1e) exhibit strong peaks near 557 nm and 412 nm at normal incidence, which correspond to the green color and blue color. The maximal reflectance values of green scales and blue scales are less than 25% and 11%, respectively. It is obvious that the antireflective properties of blue scales are much better than that of green scales. According to the result of pretreatment experiment (Experimental Section), these bright colors arise not from pigments but from self-organized ultrafine hierarchical structures in the wing scales. So the antireflective properties are structure-based instead of pigment-based.

Further, FESEM images of the blue scales under different magnifications were achieved (**Figure 2**). Interestingly, it is found that the blue scales with 3D ultrafine hierarchical structures are bilayer with two entirely different scale types. The top layer is covered with loosely aligned oval scales called cover scales (CS). On the bottom layer, scales with serrate ends lying beneath the gaps between two adjacent CS are called ground scales (GS). Moreover, CS and GS are both arranged in alternate rows and overlap with each other in a precise and repeated pattern (Figure 2a,b). The density of the scales varies from around 60 to 70 scales mm^{-2}. In fact, the array of scales plays the role of a very efficient optical diffuser over the visible range and ultrafine hierarchical structures lead to significant interactions with incident light, which eventually result in the visible blue color from certain angles. Specifically, the individual CS is about 100 μm in length and 40 μm in width (Figure 2c), while the individual GS with sharp serrate ends looks like much shorter and broader (Figure 2b). The roots of both CS and GS obliquely insert into the wing membrane that is translucent and less than 1 μm in thickness (Figure S1, Supporting Information). In fact, the join between scales and wing membrane is so weak that the aged scales can easily fall off to help butterfly generate reborn scales. In this way, high antireflective efficiency of blue scales can be maintained for long. Herein, these primary structures of CS and GS are called tower strucetures and honeycomb structures respectively for the sake of simplicity. More exquisite secondary structures of CS and GS were observed under high magnifications (Figure 2e,f). The CS surfaces consist of abundant raised parallel lamella ridges that extend along the length of the scales (inset in Figure 2e). The horizontal spacing between two adjacent ridges is 826 nm and the ridge with wavy edges is 541 nm in width. In addition, there distribute plentiful holes in a random way at the bottom of the spacing (Figure 2e). Similarly, GS surfaces are covered with sparse raised parallel comb stacks, which extend along the length of the scales as well. The combs overlap each other in turn with 324 nm in width. The horizontal spacing between two adjacent comb stacks is more than 2 μm, which is much broader than that of CS. The cross-linked ribs connect adjacent comb stacks and form dense irregular meshes, the diameters of which vary from 0.1 to 1.2 μm. It is well understood that these meshes may contribute to making light through to decrease reflection and reducing the weight of butterfly wings to lighten the load of flying as well. In addition, the lateral views of GS and CS under high magnifications have also been obtained to show these ultrafine structures more clearly (Figure 2g,h).

According to the feature sizes of the original blue scales (Table S1, Supporting Information), simplified 3D models imitating the nanostructures of CS and GS were built to further reveal their possible antireflective mechanisms (Figures S2 and S3, Supporting Information). For CS with tower structures, ridges originating from multiple lamellae and the spacing between two adjacent ridges form two different types of natural trapezoidal light trappers (TLTs) that together give full play to the role of light trapping structures. When incident lights irradiate into the TLTs region, gradient refractions and multiple Fresnel reflections based on Snell's law and the law of reflection respectively occur on air-chitin interfaces. As a result, most incident lights are trapped into the TLTs. In the meantime, the multiple Fresnel reflections tremendously increase optical path and lead to optical losses that furtherly reduce even eliminate reflections. The whole periodic tower structures formed by ridges and the spacing between them act as a blazed grating, which lead to destructive interference. Besides, there exist a surprising number of sub-300 nm scattering sites on the top of the multistacked structures, which provide a foundation for Rayleigh scattering to reinforce its antireflective effect. For GS with

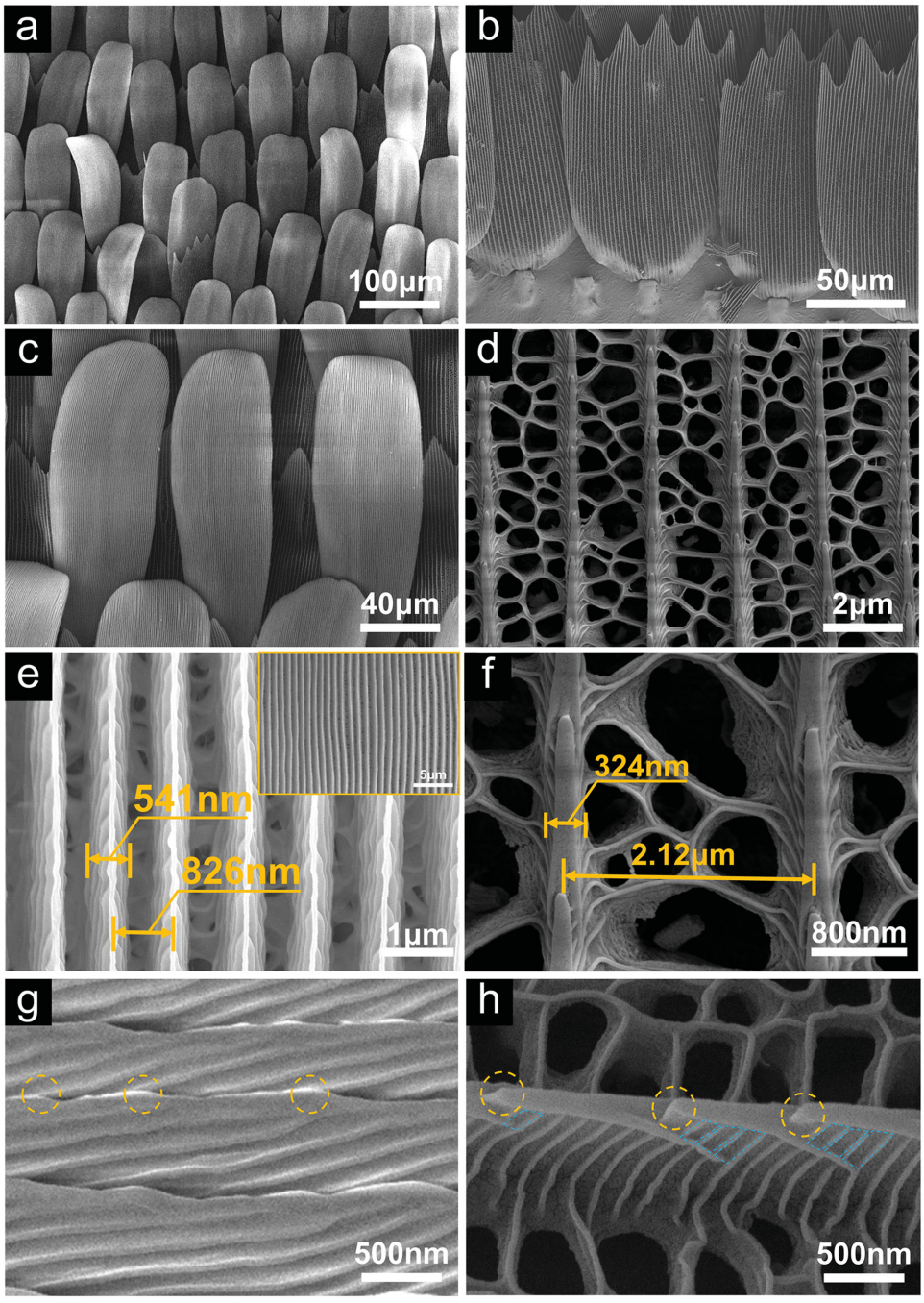

Figure 2. FESEM images of CS and GS under different magnifications. a,b) Low magnification FESEM images of CS distributing in fluffy order and GS with quasi-serrature edges; c,d) CS and GS under medium magnification show their primary structures; e) CS under high magnification presents raised ridges (inset) and parallel lamellae; f) GS under high magnification demonstrates exquisite secondary nanostructures including plentiful meshes and comb stacks; g) lateral view of lamella ridges in CS demonstrates scattering sites (orange dashed circles); h) lateral view of comb stacks in GS demonstrates scattering sites (orange dashed circles) and semi-open microcavities (blue dashed boxes).

honeycomb structures, because of sparse distribution of the raised parallel comb stacks, most parallel beam falls into the serried meshes when it transmits through the spacing between two adjacent comb stacks, which produces pinhole diffractions and enhances the transmittance of incident light to a great extent. In addition, with the aid of plentiful semi-open microcavities formed by adjacent combs, oscillations of the reflected light will continue until the reflectance falls to zero with optical losses. Meanwhile, the multilayer destructive interference and Rayleigh scattering are simultaneous on air-chitin interfaces. It is the ingenious bilayer (CS and GS) 3D ultrafine hierarchical structures including primary structures and secondary structures in butterfly wing scales that produce a combination of multiple optical effects, such as gradient refraction, multiple Fresnel reflection, pinhole diffraction, Rayleigh scattering, and multilayer destructive interference, which function together as a natural optimized multiple antireflective system.

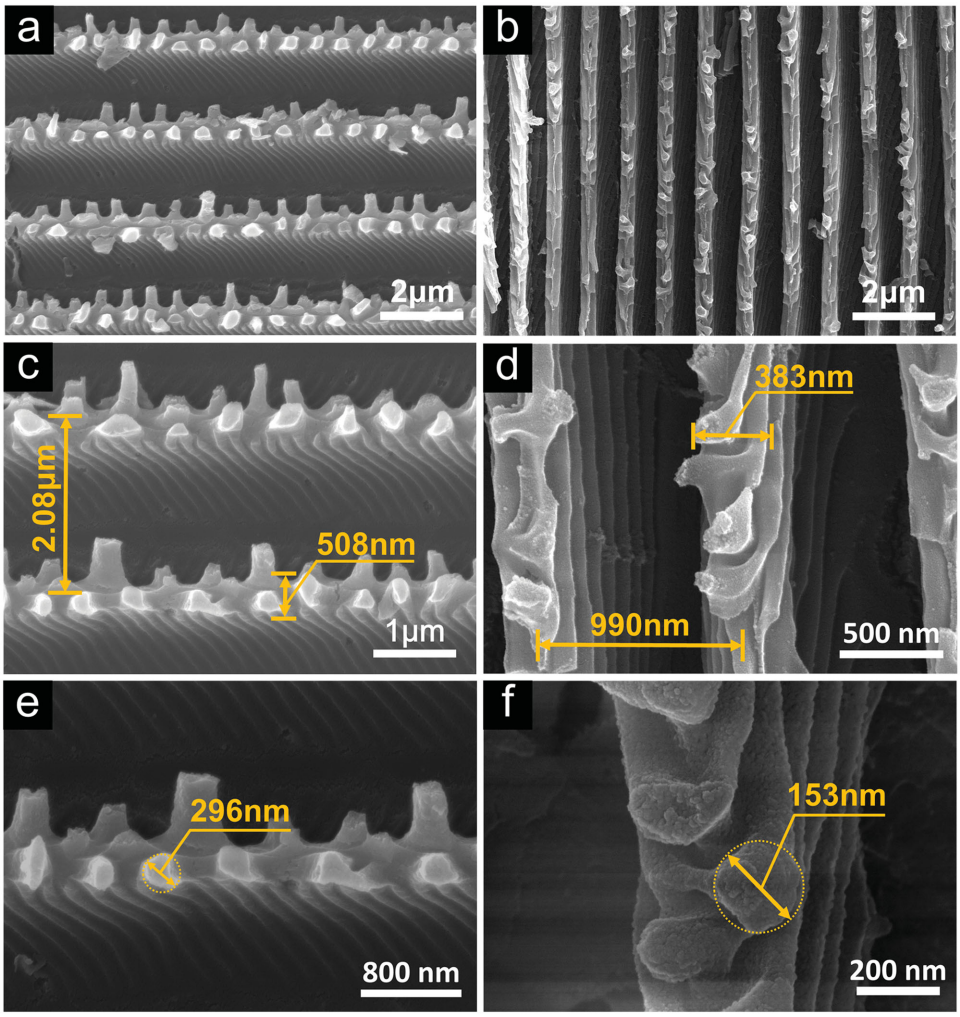

Figure 3. Different magnification FESEM images of GS replicas and CS replicas. a,b) Low-magnification FESEM images of the biomimetic replicas demonstrate periodic ordered nanoditch array structures; c,d) medium-magnification FESEM images of the feature structures of GS and CS replicas; e,f) high-magnification FESEM images of the subwavelength papilla-like structures of GS and CS replicas.

To obtain the biomimetic antireflective replicas, a low-cost and effective wet chemical biomimetic fabrication method combining sol–gel and selective etching processes was applied in this work. First, a clean slice of original wing was pretreated by diethyl ether and ethanol absolute for 10 min respectively. Then, it could be fully transformed into activated wing, which could more easily combine the hydrolysate of tetraethyl orthosilicate (TEOS) (Figure S4a–d, Supporting Information). The pretreatment could not change the exquisite nanostructures of original wing scales. More importantly, more chemical groups were exposed just as shown in the Fourier transform infrared spectroscopy (FTIR) (Figure S4e, Supporting Information), which is conducive to subsequent sol–gel process. The schematic diagram of the clear and concise fabrication process using blue scales as bio-template was briefly prepared and illustrated in detail as shown in Figure S5 (Supporting Information). The forming mechanism of the nanoditch array structures in the biomimetic replicas was explained as shown in Figure S6 (Supporting Information). It should be noted that the ultimate quality of the biomimetic replicas greatly depend on the critical sol–gel process.

Satisfyingly, the delicate colors of the biomimetic replicas based on glass substrate are not only visible with naked eyes but also possess the distinct characteristic of orientation dependence (Figure S7, Supporting Information). Thus, a preliminary deduction is that the biomimetic replicas basically inherit the optical structures in blue scales. To further evaluate quality of the biomimetic replicas, FESEM and TEM were used to characterize their morphologies and dimensions. The biomimetic replicas with scaly shape are found, which correspond to the original blue scales. Both GS replicas and CS replicas are equipped with periodic ordered nanoditch array structures along the length of the replicas (**Figure 3**a,b). However, there are distinct differences about their nanoditch array structures by crosswise comparison with each other. For GS replicas, the raised stacks with isoclinal fold stripes on the side wall and papilla-like structures atop the stacks arrange in order. A few tiny cracks caused by structural shrinkage appear in the bottom of the ditches. The width of these stacks is 508 nm and the spacing between two adjacent stacks is 2.08 μm (Figure 3c). In contrast, CS replicas were consisted of raised ridges with almost horizontal

lamellae and papilla-like structures atop the ridges. The width of these ridges is 383 nm and the spacing between two adjacent lamellae is 990 nm, which is much narrower than that of GS replicas (Figure 3d). In particular, it should be noted that the sub-300 nm papilla-like structures of GS replicas are all staggered atop the raised ridges (Figure 3e and Figure S8 in the Supporting Information), while the sub-200 nm papilla-like structures of CS replicas are hemispherical and look like much slippery (Figure 3f). In this regard, subwavelength papilla-like structures are typical ARS to dramatically suppress the reflection losses and increase transmission of light at the interfaces simultaneously over a large range of wavelengths and views.[2] The underlying formation mechanism for these papilla-like structures is that the precursor solution infiltrates into the holes and meshes in original blue scales and gradually solidify during the heating process. Subsequently, the organic scales are removed in mixed acid at high temperature via selective etching process and the final subwavelength papilla-like structures were obtained.

It can be seen from the energy dispersive spectroscopy (EDS) of the biomimetic replicas that the dominant peaks are silicon (Si) and oxygen (O) (**Figure 4**a), which confirms that the original blue scales was almost burnt out and the main compositions of the biomimetic replicas (inset in Figure 4a) are Si and O (Table S2, Supporting Information). In addition, the element enrichment regions of Si (Figure 4b) and O (Figure 4c) in the area scanning maps are consistent with the shape of the biomimetic replicas, which further indicates that high purity SiO_2 replicas were obtained.

Then, the antireflective properties and high transmission of the biomimetic replicas based on glass substrate (Figure 4d, inside rectangular box) were characterized by the reflectance and transmittance spectra (Figure 4e) over a range of wavelengths 350–900 nm. After a thorough comparative analysis, the reflection peak of the biomimetic replicas (19.78%, 390 nm) appears over a range of wavelengths 350–480 nm and has a blueshift from 412 nm to 390 nm when comparing with that of original blue scales. In so far as we can see, it may be the multilayer film interference that arouses the blueshift of the reflection peak.[26] This is consistent with the existence of multicomb structures consisting of alternating chitin and air spacer layers in original blue scales. The reflectance of the biomimetic replicas is less than 2.8% over a broad range of wavelengths (480–900 nm), which is lower than that of glass substrate (8.32%) and original blue scales (5.68%). It indicates that the excellent antireflective properties of the biomimetic replicas. Moreover, the transmittance of the biomimetic replicas is up to 95.61% over a range of wavelengths 440–900 nm, which is higher than that of glass substrate (90.19%) and original blue scales (25.16%). It confirms that the biomimetic replicas possess high transmission. And two main factors result in the high transmission. On one hand, the glass substrate made up of SiO_2 are almost transparent itself. On the other hand, the nanoditch array structure of the biomimetic replicas, a kind of open structure, is conducive to the transmission of light. Apparently, high transmission can extremely reduce the reflection and then enhance antireflective effect of the biomimetic replicas. In addition, it can be found that the biomimetic replicas are of lower transmittance at short wavelengths (350–420 nm) and the corresponding transmittance is less than 67.39%. Then the transmittance climbs sharply to 95.54% over a range of wavelengths 420–440 nm. Beyond the inherent UV absorption property of glass substrate itself (cyan solid line), one explanation for this finding is that the short wavelengths are near to the size of subwavelength papilla-like structures, which is conducive to scattering the UV and blue light to reduce the transmittance. The transmittance spectrum of blue scales was also obtained to compare the differences between biological prototype and biomimetic replicas. The maximum transmittance of blue scales is less than 25%, which is far lower than that of the SiO_2 biomimetic replicas. This is exactly consistent with our previous work on light trapping structures in blue scales of butterfly *Trogonoptera brookiana*.[27] The nanostructures in blue scales were proved to possess an excellent light trapping effect, resulting in the low transmittance of the blue scales.

To further reveal the mechanism of high-performance multiple antireflective properties of the biomimetic replicas, a brief schematic diagram (Figure 4f) was prepared to illustrate the concurrent multiple optical synergetic effects on the interfaces of papilla-like structures and multilayer structures. On one hand, after experience gradient refractions in multilayer structures (Figure 4f, left) and multiple reflections between adjacent papilla-like structures (Figure 4f, middle), light path markedly increases to make for light absorption and incident lights acquire a more complicated polarization state.[28] The polarization state mainly depends on where the incident lights hit on the interfaces and determines the form of interference: constructive or destructive interference. Generally, the constructive interference can be described by the relation as follows

$$\lambda \propto 2d_{\text{eff}}\sqrt{n_{\text{eff}} - \sin^2\theta} \tag{1}$$

where λ is constructive wavelength, d_{eff} is the whole film thickness, n_{eff} is the effective refractive index of the SiO_2 and air-spacer multilayers, and θ is the angle of incidence (0° here). According to Equation (1), it is obvious that λ will vary and the biomimetic replicas can present different colors with the change of corresponding θ. On the other hand, Rayleigh scattering presenting on the interfaces is attributed to the subwavelength size effect of papilla-like structures (Figure 4f, right), which also contributes to further reducing reflection. And the relationship between light intensity of Rayleigh scattering (I_s) and wavelength of incident light (λ_i) can be described qualitatively as follows:

$$I_s \propto \frac{I_i}{\lambda_i^4} \tag{2}$$

where I_i is the intensity of incident light. According to Equation (2), short wave is more easily scattered than long wave and then it is well understood why the biomimetic replicas present delicate blue color (400–480 nm). Thus, it is these multiple optical synergetic effects acting on the interfaces that realize high-performance multiple antireflection of the biomimetic replicas. Also, there is a good agreement between the original blue scales and the biomimetic replicas. So, both

www.MaterialsViews.com

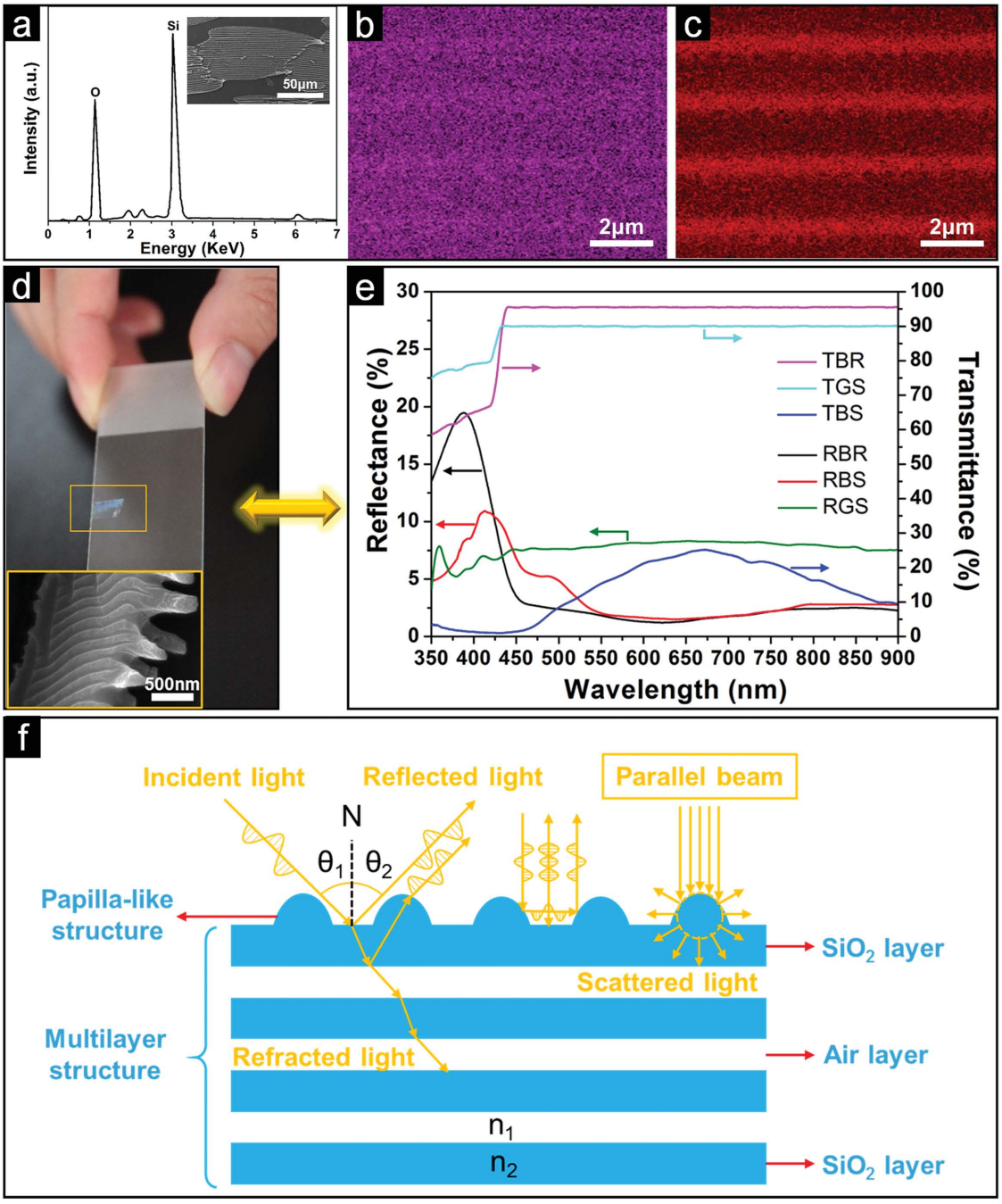

Figure 4. a) EDS of the fabricated biomimetic replicas shows the main elements: Si and O; b,c) scanning maps demonstrate the distributions of Si and O respectively, which are consistent with the shapes of the antireflective nanoditch array structures; d) photograph and high-magnification FESEM image (inset) of biomimetic replicas (a near 1 cm^2 rectangular region) exhibit delicate blue color and the pore-free surface, respectively; e) reflectance and transmittance spectra of biomimetic replicas (RBR and TBR), blue scales (RBS and TBS), and glass substrate (RGS and TGS); f) schematic description of the antireflective mechanism of biomimetic replicas. Herein, ***N*** is a normal, θ_1 and θ_2 ($\theta_2 = \theta_1$) are the angles of incidence and reflection respectively, n_1 (1.00) and n_2 (1.45) are the refractive indices of air and SiO_2 respectively.

the photonic nanostructures and the antireflective properties of the original blue scales were well-preserved by the biomimetic replicas.

In summary, the high-performance structure-based antireflective properties of the blue scales in butterfly *Trogonoptera brookiana* wings were found. The multiple antireflective mechanism of the original blue scales had been fully revealed. It is found that the bilayer 3D ultrafine hierarchical structures in blue scales play a vital role in realizing multiple antireflection. Taking inspiration from the blue scales, biomimetic replicas with antireflective nanoditch array structures had been fabricated successfully on glass substrate using a facile wet chemical biomimetic fabrication method. It was confirmed that the fabricated SiO_2 biomimetic replicas inherit not only the bilayer 3D ultrafine hierarchical structures effectively but also the high-performance multiple antireflective

properties of original wing scales. What is more, the multiple antireflective mechanism of the SiO_2 biomimetic replicas was elaborated. And it is believed that multiple optical synergetic effects including multiple refraction, destructive interference, Rayleigh scattering of papilla-like structures and gradient refraction of multilayer structures acting on respective interfaces realize the high-performance antireflection of the biomimetic replicas. In terms of the antireflective properties and high transmission, the fabricated SiO_2 biomimetic replicas as antireflective surfaces demonstrate a promising potential for extensive applications in optoelectronic equipment to improve device performance, such as LED, solar cells, optical elements, etc. Further, the proposed method may provide a promising strategy for accurately manufacturing the known natural ultrafine 3D nanostructures. As such, this work could probably inspire engineers to develop novel functional surfaces with unique structures for practical applications.

Experimental Section

Biological Prototype: The green scales and blue scales of male butterfly *Trogonoptera brookiana* (Alfred R. Wallace, 1855) (family: *Papilionini*) wings were taken as experimental materials to do further research.

Pretreatment Experiment: A simple discoloration experiment was carried out to confirm that the color of the wing scales is structure-based rather than pigments. First, the neat and clean green and blue areas were cut off the right fore wing meticulously with a scalpel in perpendicular and parallel directions to the nervure, respectively. Then, the specimen was clamped with a tweezer to flatwise place in a petri dish and soaked into a certain amount of diethyl ether and ethanol absolute for 10 min respectively to increase the mechanical strength of the wing tissues. The color of the air dried specimen was still brilliant, which was not affected by organic solvents virtually. Diethyl ether and ethanol absolute were provided by Tianjin Fuyu Fine Chemical Co., Ltd. All reagents used in this experiment were of analytical grade (A. R.) without further purification.

Fabrication Method: The SiO_2 biomimetic replicas were fabricated using a facile wet chemical biomimetic fabrication method combining sol–gel and selective etching processes as shown in Figure S7 (Supporting Information). The fabricated biomimetic replicas were preserved in a slide box. Concentrated nitric acid (A. R.) and TEOS were provided by Beijing Chemical Works, perchloric acid and hydrochloric acid were provided by Changchun Hongyu Chemical Co., Ltd.

Characterization: In order to achieve the FTIR spectra of original wing and activated wing using a Bruker EQUINOX 55 instrument, the samples were mashed to powder and compressed into KBr (A. R.) pellets. With the help of 3D stereoscopic microscope (KEYENCE VHX-5000) and ultrahigh resolution FESEM (ZEISS MERLIN Compact), the morphologies and dimensions of blue scales and biomimetic replicas were characterized under different magnifications. And the EDS (OXFORD X-Max^N 150) was used to confirm the composition and distribution of the elements in the SiO_2 biomimetic replicas. The reflectance spectra and transmittance spectra of original wing scales and biomimetic replicas were obtained using a miniature fiber optic spectrometer (Ocean Optics USB 4000). Herein, the spot size of the incident beam was 5 mm in diameter. And the spectrometer was carefully calibrated with a standard white board STD-WS that was certified by the National Institute of Metrology of China and a standard glass under R model and T model, respectively.

Supporting Information

Supporting Information is available from the Wiley Online Library or from the author.

Acknowledgements

This work was supported by the National Natural Science Foundation of China (Nos. 51325501, 51505183, 51175220, and 51290292), and China Postdoctoral Science Foundation Funded Project (No. 2015M571360).
These acknowledgements were updated on February 10, 2016.

[1] a) J. Zhu, C. M. Hsu, Z. Yu, S. Fan, Y. Cui, *Nano Lett.* **2009**, *10*, 1979; b) F. Llopis, I. Tobías, *J. Appl. Phys.* **2006**, *100*, 124504.
[2] Y. Li, J. Zhang, B. Yang, *Nano Today* **2010**, *5*, 117.
[3] H. K. Raut, A. S. Nair, S. S. Dinachali, V. A. Ganesh, T. M. Walsh, S. Ramakrishna, *Sol. Energy Mater. Sol. Cells* **2013**, *111*, 9.
[4] T. Druffel, K. Geng, E. Grulke, *Nanotechnology* **2006**, *17*, 3584.
[5] J. A. Hiller, J. D. Mendelsohn, M. F. Rubner, *Nat. Mater.* **2002**, *1*, 59.
[6] a) J. Cai, J. Ye, S. Chen, X. Zhao, D. Zhang, S. Chen, Y. Ma, S. Jin, L. Qi, *Energy Environ. Sci.* **2012**, *5*, 7575; b) H. K. Raut, V. A. Ganesh, A. S. Nair, S. Ramakrishna, *Energy Environ. Sci.* **2011**, *4*, 3779; c) S. A. Boden, D. M. Bagnall, *Appl. Phys. Lett.* **2008**, *93*, 133108; d) C. H. Sun, P. Jiang, B. Jiang, *Appl. Phys. Lett.* **2008**, *92*, 061112; e) P. Clapham, M. Hutley, *Nature* **1973**, *244*, 281.
[7] J. Huang, X. Wang, Z. L. Wang, *Nanotechnology* **2008**, *19*, 025602.
[8] G. Zhang, J. Zhang, G. Xie, Z. Liu, H. Shao, *Small* **2006**, *2*, 1440.
[9] a) S. Niu, B. Li, Z. Mu, M. Yang, J. Zhang, Z. Han, L. Ren, *J. Bionic Eng.* **2015**, *12*, 170; b) Z. Han, S. Niu, W. Li, L. Ren, *Appl. Phys. Lett.* **2013**, *102*, 233702; c) S. Lou, X. Guo, T. Fan, D. Zhang, *Energy Environ. Sci.* **2012**, *5*, 9195; d) Q. Zhao, X. Guo, T. Fan, J. Ding, D. Zhang, Q. Guo, *Soft Matter* **2011**, *7*, 11433; e) D. G. Stavenga, S. Foletti, G. Palasantzas, K. Arikawa, *Proc. R. Soc. London, Ser. B* **2006**, *273*, 661.
[10] a) D. Zhang, W. Zhang, J. Gu, T. Fan, Q. Liu, H. Su, S. Zhu, *Prog. Mater. Sci.* **2015**, *68*, 67; b) Z. Han, S. Niu, L. Zhang, Z. Liu, L. Ren, *J. Bionic Eng.* **2013**, *10*, 162; c) G. Sun, Y. Fang, Q. Cong, L. Ren, *J. Bionic Eng.* **2009**, *6*, 71.
[11] a) X. Wang, Y. Liao, B. Liu, L. Ge, G. Li, S. Fu, Y. Chen, Z. Cui, *Microelectron. Eng.* **2008**, *85*, 910; b) Y. Kanamori, E. Roy, Y. Chen, *Microelectron. Eng.* **2005**, *78*, 287.
[12] a) K. S. Han, J. H. Shin, W. Y. Yoon, H. Lee, *Sol. Energy Mater. Sol. Cells* **2011**, *95*, 288; b) K. S. Han, J. H. Shin, H. Lee, *Sol. Energy Mater. Sol. Cells* **2010**, *94*, 583; c) G. Xie, G. Zhang, F. Lin, J. Zhang, Z. Liu, S. Mu, *Nanotechnology* **2008**, *19*, 095605; d) L. J. Guo, *Adv. Mater.* **2007**, *19*, 495.
[13] Y. M. Song, S. Y. Bae, J. S. Yu, Y. T. Lee, *Opt. Lett.* **2009**, *34*, 1702.
[14] a) H. Sai, H. Fujii, K. Arafune, Y. Ohshita, M. Yamaguchi, Y. Kanamori, H. Yugami, *Appl. Phys. Lett.* **2006**, *88*, 201116; b) Y. Kanamori, K. Hane, H. Sai, H. Yugami, *Appl. Phys. Lett.* **2001**, *78*, 142.

[15] a) Y. Li, J. Zhang, S. Zhu, H. Dong, F. Jia, Z. Wang, Z. Sun, L. Zhang, Y. Li, H. Li, W. Xu, B. Yang, *Adv. Mater.* **2009**, *21*, 4731; b) H. Chen, S. Chuang, C. Lin, Y. Lin, *Opt. Express* **2007**, *15*, 14793.
[16] a) Y. Hung Jr., S. L. Lee, L. A. Coldren, *Opt. Express* **2010**, *18*, 6841; b) T. Lohmüller, M. Helgert, M. Sundermann, R. Brunner, J. P. Spatz, *Nano Lett.* **2008**, *8*, 1429.
[17] a) J. Leem, D. Joo, J. Yu, *Sol. Energy Mater. Sol. Cells* **2011**, *95*, 2221; b) Y. Li, J. Zhang, S. Zhu, H. Dong, F. Jia, Z. Wang, Y. Tang, L. Zhang, S. Zhang, B. Yang, *Langmuir* **2010**, *26*, 9842; c) Y. M. Song, S. J. Jang, J. S. Yu, Y. T. Lee, *Small* **2010**, *6*, 984.
[18] a) C. H. Hsu, H. C. Lo, C. F. Chen, C. T. Wu, J. S. Hwang, D. Das, J. Tsai, L. C. Chen, K. H. Chen, *Nano Lett.* **2004**, *4*, 471; b) C. Hsu, Y. Huang, L. Chen, S. Chattopadhyay, K. Chen, H. Lo, C. Chen, *J. Vac. Sci. Technol., B* **2006**, *24*, 308; c) S. Chattopadhyay, L. C. Chen, K. H. Chen, *Crit. Rev. Solid State Mater. Sci.* **2006**, *31*, 15.
[19] a) S. L. Diedenhofen, G. Vecchi, R. E. Algra, A. Hartsuiker, O. L. Muskens, G. Immink, E. P. Bakkers, W. L. Vos, J. G. Rivas, *Adv. Mater.* **2009**, *21*, 973; b) Y. J. Lee, D. S. Ruby, D. W. Peters, B. B. McKenzie, J. W. Hsu, *Nano Lett.* **2008**, *8*, 1501; c) H. Y. Chen, H. W. Lin, C. Y. Wu, W. C. Chen, J. S. Chen, S. Gwo, *Opt. Express* **2008**, *16*, 8106; d) J. Q. Xi, M. F. Schubert, J. K. Kim, E. F. Schubert, M. Chen, S. Y. Lin, W. Liu, J. A. Smart, *Nat. Photonics* **2007**, *1*, 176; e) J. Q. Xi, J. K. Kim, E. Schubert, D. Ye, T. M. Lu, S. Y. Lin, J. S. Juneja, *Opt. Lett.* **2006**, *31*, 601.
[20] a) X. Zhao, B. Sanchez, P. Dobson, *Nanoscale* **2011**, *3*, 839; b) M. Geissler, Y. Xia, *Adv. Mater.* **2004**, *16*, 1249.
[21] a) C. Lin, J. Shieh, C. Liang, C. Cheng, Y. Chen, *J. Mater. Chem. C* **2014**, *2*, 3645; b) H. J. Gwon, Y. Park, C. W. Moon, S. Nahm, S. J. Yoon, S. Y. Kim, H. W. Jang, *Nano Res.* **2014**, *7*, 670; c) S. Ravipati, J. Shieh, F. H. Ko, C. C. Yu, H. L. Chen, C. T. Wu, S. H. Chen, *Energy Environ. Sci.* **2012**, *5*, 7601; d) J. Shieh, C. Lin, M. Yang, *J. Phys. D: Appl. Phys.* **2007**, *40*, 2242.
[22] a) M. Toma, G. Loget, R. M. Corn, *Nano Lett.* **2013**, *13*, 6164; b) Y. Wang, Z. Zeng, J. Li, L. Chi, X. Guo, N. Lu, *J. Am Soc. Mass Spectrom.* **2013**, *24*, 66; c) K. X. Wang, Z. Yu, V. Liu, Y. Cui, S. Fan, *Nano Lett.* **2012**, *12*, 1616; d) S. H. Lee, G. E. Jellison Jr., C. E. Duty, J. Xu, *Appl. Phys. Lett.* **2011**, *99*, 153113; e) M. Peres, M. Soares, A. Neves, T. Monteiro, V. Sandana, F. Teherani, D. Rogers, *Phys. Status Solidi B* **2010**, *247*, 1695; f) J. Zhu, Z. Yu, G. F. Burkhard, C. M. Hsu, S. T. Connor, Y. Xu, Q. Wang, M. McGehee, S. Fan, Y. Cui, *Nano Lett.* **2008**, *9*, 279.
[23] a) M. Sun, A. Liang, Y. Zheng, G. S. Watson, J. A. Watson, *Bioinspiration Biomimetics* **2011**, *6*, 026003; b) C. H. Sun, W. L. Min, N. C. Linn, P. Jiang, B. Jiang, *Appl. Phys. Lett.* **2007**, *91*, 231105; c) P. Papet, O. Nichiporuk, A. Kaminski, Y. Rozier, J. Kraiem, J. F. Lelievre, A. Chaumartin, A. Fave, M. Lemiti, *Sol. Energy Mater. Sol. Cells* **2006**, *90*, 2319; d) H. Sai, H. Fujii, K. Arafune, Y. Ohshita, M. Yamaguchi, Y. Kanamori, H. Yugami, *Appl. Phys. Lett.* **2006**, *88*, 201116.
[24] a) J. Zhu, Y. K. Sharma, Z. Zeng, X. Zhang, M. Srinivasan, S. Mhaisalkar, H. Zhang, H. H. Hng, Q. Yan, *J. Phys. Chem. C* **2011**, *115*, 8400; b) Z. Lu, Z. Chang, W. Zhu, X. Sun, *Chem. Commun.* **2011**, *47*, 9651; c) B. Varghese, M. Reddy, Z. Yanwu, C. S. Lit, T. C. Hoong, G. Subba Rao, B. Chowdari, A. T. S. Wee, C. T. Lim, C. H. Sow, *Chem. Mater.* **2008**, *20*, 3360.
[25] R. A. Potyrailo, H. Ghiradella, A. Vertiatchikh, K. Dovidenko, J. R. Cournoyer, E. Olson, *Nat. Photonics* **2007**, *1*, 123.
[26] a) Z. Zhang, K. Yu, L. Lou, H. Yin, B. Li, Z. Zhu, *Nanoscale* **2012**, *4*, 2606; b) P. Vukusic, R. Sambles, C. Lawrence, G. Wakely, *Appl. Opt.* **2001**, *40*, 1116.
[27] Z. Han, S. Niu, C. Shang, Z. Liu, L. Ren, *Nanoscale* **2012**, *4*, 2879.
[28] a) S. Mahajan, J. J. Baumberg, U. Steiner, *Nat. Nanotechnol.* **2010**, *5*, 511; b) S. Coyle, G. V. Prakash, J. Baumberg, M. Abdelsalem, P. Bartlett, *Appl. Phys. Lett.* **2003**, *83*, 767.

Received: August 15, 2015
Revised: October 28, 2015
Published online: December 20, 2015